DØ Note 5504-CONF

Combined Upper Limits on Standard Model Higgs Boson Production from the DØ Experiment in 0.9-1.7 fb^{-1}

The DØ Collaboration
URL http://www-d0.fnal.gov
(Dated: December 7, 2007)

Upper limits on the cross section for standard model Higgs boson production in $p\bar{p}$ collisions at $\sqrt{s} = 1.96$ TeV are determined for Higgs masses (m_H) in the range $105 < m_H < 200$ GeV/c^2. The contributing production processes include associated production ($WH \to \ell\nu b\bar{b}$, $ZH \to \ell\ell/\nu\nu b\bar{b}$, $WH \to WW^+W^-$) and gluon fusion ($H \to W^+W^-$). Analyses are conducted with integrated luminosities from 0.9 fb^{-1} to 1.7 fb^{-1} recorded by the DØ experiment. The results are in good agreement with background expectations and the observed 95% C.L. upper limits are found to be a factor of 6.4 (2.6) higher than the standard model cross section at m_H =115 (160) GeV/c^2while the expected limits are found to be a factor of 5.8 (2.8) higher than the standard model cross section for the same masses.

I. INTRODUCTION

Despite its success as a predictive tool, the standard model (SM) of particle physics remains incomplete without a means to explain electroweak symmetry breaking. The simplest proposed mechanism involves the introduction of a complex doublet of scalar fields that generate particle masses via their mutual interactions. After accounting for longitudinal polarizations for the electroweak bosons, this so-called Higgs mechanism also gives rise to a single scalar boson with an unpredicted mass. Direct searches in $e^+e^- \to Z^* \to ZH$ at the Large Electron Positron (LEP) collider yielded lower mass limits at $m_H > 114.4$ GeV/c^2 [1] while precision electroweak data yield the indirect constraint $m_H < 144$ GeV/c^2 [2], with both limits set at 95% C.L. The SM Higgs boson search is one of the main goals of the Fermilab Tevatron physics program.

In this note, we combine recent results for direct searches for SM Higgs bosons in $p\bar{p}$ collisions at $\sqrt{s} = 1.96$ TeV recorded by the DØ experiment [3]. These are searches for Higgs bosons produced in association with vector bosons ($p\bar{p} \to W/ZH \to \ell\nu/\ell\ell/\nu\nu b\bar{b}$ and $p\bar{p} \to WH + X \to WW^+W^-$) or singly through gluon-gluon fusion ($p\bar{p} \to H + X \to W^+W^-$). The searches were conducted with data collected during the period 2002-2007 and correspond to integrated luminosities ranging from 0.9 fb^{-1} to 1.7 fb^{-1}. The searches are organized into fifteen final states, each designed to isolate a particular Higgs boson production and decay mode. In order to facilitate proper combination of signals, the analyses were designed to be mutually exclusive after analysis selections. Searches for several final states are performed in two distinct epochs of data collection: before and after the 2006 DØ detector upgrade. The largest changes made during the upgrade were the addition of a new layer to the silicon detector nearest to the beam-line and an upgrade of the trigger system. The two epochs are denoted as Run IIa (1.1fb^{-1}) and Run IIb(0.6fb^{-1}). This results in a total of 23 individual analyses.

The 23 analyses [4–10] are outlined in Table I. In the cases of $p\bar{p} \to W/ZH + X$ production, we search for a Higgs boson decaying to two bottom-quarks. The decays of the vector bosons further define the analyzed final states: $WH \to \ell\nu b\bar{b}$, $ZH \to \ell\ell b\bar{b}$ and $ZH \to \nu\bar{\nu}b\bar{b}$. In order to isolate $H \to b\bar{b}$ decays, an algorithm for identifying jets consistent with the decay of a heavy-flavor quark is applied to each jet. Several kinematic variables senstive to transversely-displaced jet track vertices and jet tracks with large transverse impact parameters relative to the hard-scatter vertes are combined in a neural network (NN) discriminant trained to indentify real heavy-flavor quark decays and reject jets arising from light-flavor quarks[11]. By adjusting a minimum requirement on the NN output, a spectrum of increasingly stringent b-tagging operating points are achieved, each with a different signal efficiency and purity. For the $WH \to \ell\nu b\bar{b}$ and $ZH \to \ell\ell b\bar{b}$ processes, the analyses are separated into two orthogonal groups: one in which two of the jets were b-tagged with a loose tagging requirement (herein called double b-tag or DT) and one group in which only one jet was tagged with a tight tag algorithm (single b-tag or ST). The $WH \to \ell\nu b\bar{b}$ analyses use tagging requirements that result in an efficiency and fake rate for signal events of about 59% and 1.5% for loose tags and about 48% and 0.5% for tight tags. The $ZH \to \ell\ell b\bar{b}$ analyses use different requirements resulting in an efficiency and fake rate of about 72% and 6% for loose tags and about 45% and 0.5% for tight tags. For these analyses, only final states with exactly two jets are selected and each lepton flavor of the W/Z boson decay ($\ell = e, \mu$) is treated as an independent channel.

For the $ZH \to \nu\bar{\nu}b\bar{b}$ analysis, two or more jets are required in the final state with two jets satisfying a loose b-tag and one of these jets also satisfying a tight b-tag. The $ZH \to \nu\bar{\nu}b\bar{b}$ analysis uses tagging requirements that result in an efficiency and fake rate for signal events of about 70% and 4.5% for loose tags and about 50% and 0.4% for tight tags. In the case of $WH \to \ell\nu b\bar{b}$ production, the primary lepton from the W boson decay may fall outside of the detector fiducial volume or is not identified. This case is treated as a separate WH analysis, referred to as $WH \to \not{\ell}\nu b\bar{b}$. For this channel, the background is the same as for the $ZH \to \nu\bar{\nu}b\bar{b}$ analysis.

We also consider Higgs decays to two $W^\pm$ bosons. For $WH \to WW^+W^-$ production, we search for leptonic W boson decays with three final states of same-signed leptons: $WWW \to e^\pm\nu e^\pm\nu + X$, $e^\pm\nu\mu^\pm\nu + X$, and $\mu^\pm\nu\mu^\pm\nu + X$. In the case of $p\bar{p} \to H + X \to W^+W^-$ production, we search for leptonic W boson decays with three final states of opposite-signed leptons: $WW \to e^+\nu e^-\nu$, $e^\pm\nu\mu^\mp\nu$, and $\mu^+\nu\mu^-\nu$. For the gluon fusion process, $H \to b\bar{b}$ decays are not considered due to the large multijets background. In all $H \to W^+W^-$ decays with $m_H < 2 \times m_W$, one of the W bosons will be off mass shell.

All Higgs signals are simulated using PYTHIA v6.202 [12] using CTEQ6L1 [13] leading order parton distribution functions. The signal cross sections are normalized to next-to-next-to-leading order (NNLO) calculations [14, 15] and branching ratios are calculated using HDECAY [16]. The contributions from QCD multijet production are measured in data. The other backgrounds were generated by PYTHIA, ALPGEN [17], and COMPHEP [18], with PYTHIA providing parton-showering and hadronization. Background cross sections are either normalized to next-to-leading order (NLO) calculations from MCFM [19] or to data control samples whenever possible.

TABLE I: List of analysis channels, corresponding integrated luminosities, and final variables. See Sect. I for details. The final variable used for several analyses is a neural-network discriminant output which is abbreviated as "NN discriminant".

Channel	Data Epoch	Luminosity (fb^{-1})	Final Variable	Reference
$WH \to \mu\nu b\bar{b}$, ST/DT	Run IIa	1.05	NN discriminant	[4]
$WH \to \mu\nu b\bar{b}$, ST/DT	Run IIb	0.63	NN discriminant	[4]
$WH \to e\nu b\bar{b}$, ST/DT	Run IIa	1.04	NN discriminant	[4]
$WH \to e\nu b\bar{b}$, ST/DT	Run IIb	0.64	NN discriminant	[4]
$WH \to \ell\nu b\bar{b}$, DT	Run IIa	0.93	NN discriminant	[5]
$ZH \to \nu\bar{\nu} b\bar{b}$, DT	Run IIa	0.93	NN discriminant	[5]
$ZH \to \mu^+\mu^- b\bar{b}$, ST/DT	Run IIa	1.10	NN discriminant	[6]
$ZH \to e^+e^- b\bar{b}$, ST/DT	Run IIa	1.10	NN discriminant	[6]
$WH \to WW^+W^-$ ($\mu^\pm\mu^\pm$)	Run IIa	1.00	2-D Likelihood	[7]
$WH \to WW^+W^-$ ($e^\pm\mu^\pm$)	Run IIa	1.00	2-D Likelihood	[7]
$WH \to WW^+W^-$ ($e^\pm e^\pm$)	Run IIa	1.00	2-D Likelihood	[7]
$H \to W^+W^-$ ($\mu^+\mu^-$)	Run IIa	1.10	NN discriminant	[8]
$H \to W^+W^-$ ($e^\pm\mu^\mp$)	Run IIa	1.10	NN discriminant	[8]
$H \to W^+W^-$ (e^+e^-)	Run IIa	1.10	NN discriminant	[8]
$H \to W^+W^-$ ($\mu^+\mu^-$)	Run IIb	0.60	NN discriminant	[8]
$H \to W^+W^-$ ($e^\pm\mu^\mp$)	Run IIb	0.64	NN discriminant	[9]
$H \to W^+W^-$ (e^+e^-)	Run IIb	0.63	NN discriminant	[10]

II. LIMIT CALCULATIONS

We combine results using the CL_s method with a log-likelihood ratio (LLR) test statistic [20]. The value of CL_s is defined as $CL_s = CL_{s+b}/CL_b$ where CL_{s+b} and CL_b are the confidence levels for the signal-plus-background hypothesis and the background-only hypothesis, respectively. These confidence levels are evaluated by integrating corresponding LLR distributions populated by simulating outcomes via Poisson statistics. Separate channels and bins are combined by summing LLR values over all bins and channels. This method provides a robust means of combining individual channels while maintaining individual channel sensitivities and incorporating systematic uncertainties. Systematics are treated as Gaussian uncertainties on the expected numbers of signal and background events, not the outcomes of the limit calculations. This approach ensures that the uncertainties and their correlations are propagated to the outcome with their proper weights. The CL_s approach used in this analysis utilizes binned final-variable distributions rather than a single-bin (fully integrated) value for each contributing analysis.

A. Final Variable Preparation

For the $WH \to \ell\nu b\bar{b}$, $ZH \to \ell\ell/\nu\nu b\bar{b}$, and $H \to W^+W^-$ analyses, the final variable used for limit setting is the output of a neural-network (NN) discriminant, trained separately for each Higgs mass tested. For the $H \to W^+W^-$ analyses, each NN is constructed using kinematic variables which may be different for each Higgs mass. The $WH \to WW^+W^-$analysis utilizes a two-dimensional likelihood discriminant as a final variable. Several background components of the final variables are smoothed via Gaussian kernel estimation [21] to minimize fluctuations in the shape of the final variable arising from limited statistics of simulated samples. Examples of the final variables for several analyses are shown in Figs. 1a-d and Figs. 2a-d, which are shown after any smoothing processes.

To decrease the granularity of the steps between simulated Higgs masses in the limit calculation, additional Higgs mass points are created via signal point interpolation [22]. The primary motivation of this procedure is to provide a means of combining analyses which do not share a common simulated Higgs mass. However, this procedure also allows a measurement of the behavior of each limit on a finer granularity than otherwise possible.

B. Systematic Uncertainties

The systematic uncertainties differ between analyses for both the signals and backgrounds [4–10]. Here we will summarize only the largest contributions. Most analyses carry an uncertainty on the integrated luminosity of 6.1%, while the overall normalization of other analyses is determined from the NNLO Z/γ^* cross section in data events

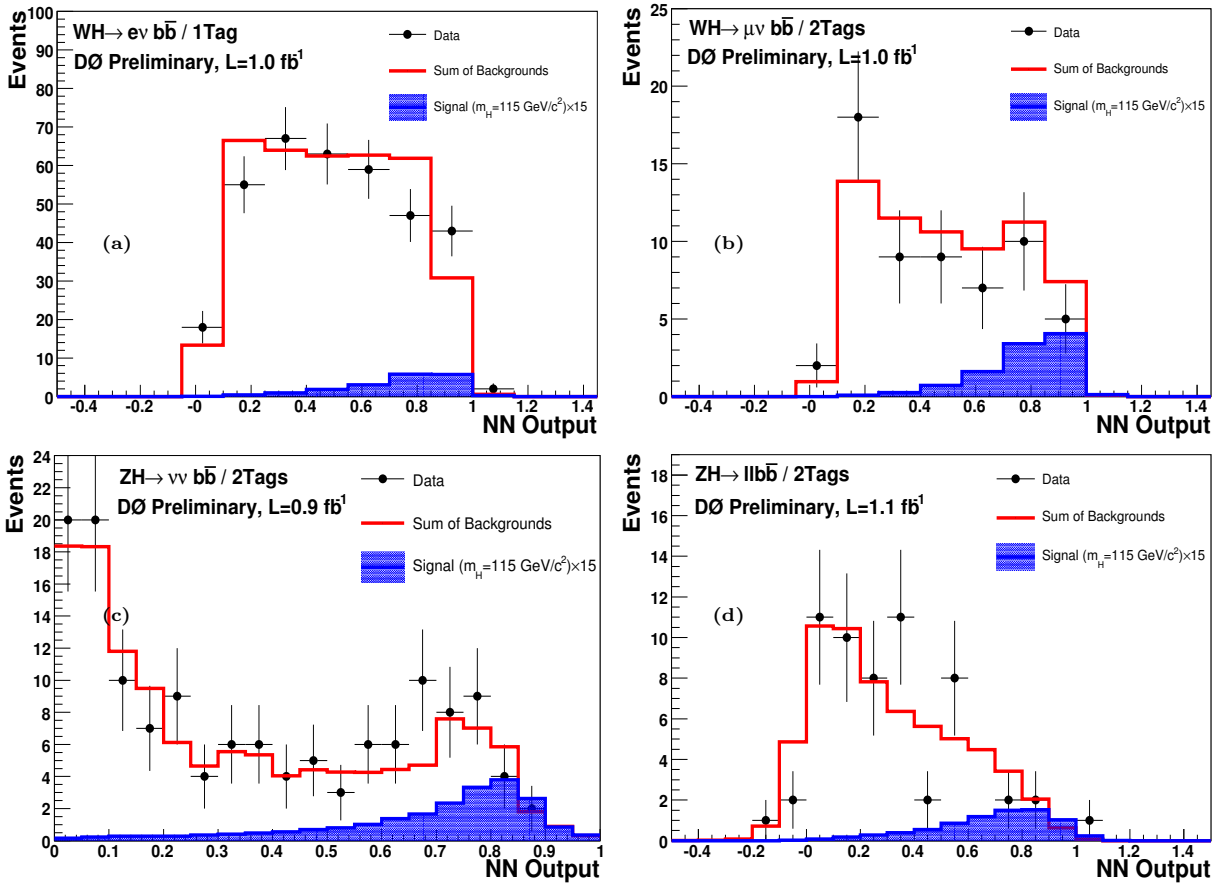

FIG. 1: Final variable distributions for selected Higgs search analyses. The figure contains distributions for: the NN discriminant for the $WH \to e\nu b\bar{b}$ ST analysis (a), the NN discriminant for the $WH \to \mu\nu b\bar{b}$ DT analysis (b), the NN discriminant for the $ZH \to \nu\bar{\nu}b\bar{b}$ DT analysis (c), the NN discriminant for the $ZH \to \ell\ell b\bar{b}$ DT analyses (d). For each figure, the total background expectations and observed data are shown. The expected Higgs signals at selected masses are scaled as indicated.

near the peak of $Z \to \ell\ell$ decays in data. The $H \to b\bar{b}$ analyses have an uncertainty on the b-tagging rate of 4-6% per tagged jet. These analyses also have an uncertainty on the jet measurement and acceptances of $\sim 7.5\%$. For the $H \to W^+W^-$ analyses we include uncertainties associated with lepton measurement and acceptances, which range from 3-6% depending on the final state. The largest contribution for all analyses is the uncertainty on the background cross sections at 6-30% depending on the analysis channel and specific background. These values include both the uncertainty on the theoretical cross section calculations and the uncertainties on the NLO→NNLO correction factors. The uncertainty on the expected multijet background is dominated by the statistics of the data sample from which it is estimated, and is considered separately from the other cross section uncertainties. The $p\bar{p} \to H + X \to W^+W^-$ analyses are also assigned a 10% uncertainty on the NNLO Higgs production cross section associated with the accuracy of the theoretical calculation. Further details on the systematic uncertainties are given in Table II.

The systematic uncertainties for background rates are generally several times larger than the signal expectation itself and are an important factor in the calculation of limits. As such, each systematic uncertainty is folded into the signal and background expectations in the limit calculation via Gaussian distribution. These Gaussian values are sampled for each Poisson trial (pseudo-experiment). Several of the systematic uncertainties, for example the jet energy scale uncertainty, impact the shape of the final variable. These shape-dependencies were preserved in the description of systematic fluctuations for each Poisson trial. Correlations between systematic sources are carried through in the calculation. For example, the uncertainty on the integrated luminosity is held to be correlated between all signals and backgrounds and, thus, the same fluctuation in the luminosity is common to all channels for a single pseudo-experiment. All systematic uncertainties originating from a common source are held to be correlated, as detailed in Tables II and III.

To minimize the degrading effects of systematics on the search sensitivity, the individual background contributions are fitted to the data observation by minimizing a profile likelihood function [23]. The fit computes the optimal

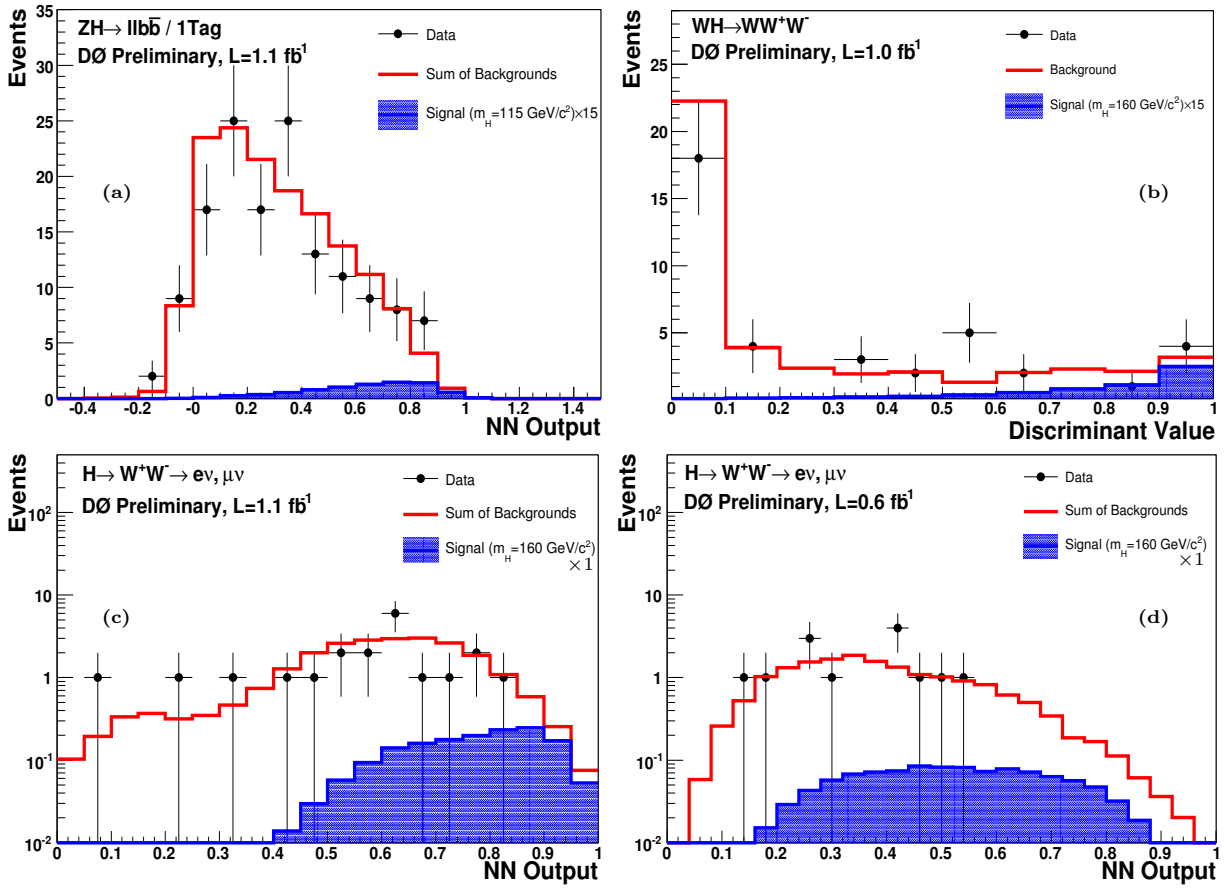

FIG. 2: Final variable distributions for selected Higgs search analyses. The figure contains distributions for: the NN discriminant for the $ZH \to \ell\ell b\bar{b}$ ST analysis (a), a one-dimensional projection of the two-dimensional likelihood for the $WH \to WW^+W^-$ analyses (b), the NN discriminant for the RunIIa $H \to W^+W^- \to e\nu, \mu\nu$ analysis (c), the NN discriminant for the RunIIb $H \to W^+W^- \to e\nu, \mu\nu$ analysis (d). For each figure, the total background expectation and observed data are shown. The expected Higgs signals are scaled as indicated.

central values for the systematic uncertainties, while accounting for departures from the nominal predictions by including a term in the χ^2 function which sums the squared deviation of each systematic in units normalized by its $\pm 1\sigma$ uncertainty. A fit is performed to the background-only hypothesis separately for each Poisson MC trial, and is constrained to bins with signal expectations less than 4% of the total expected background.

To ensure a reliable implementation, additional coverage studies are performed to ensure the accuracy of the calculation. The Frequentist coverage probability was evaluated for two masses in the hypothetical Higgs search spectrum: $m_H = 115$ GeV/c^2 and $m_H = 160$ GeV/c^2. Figures 3 shows the coverage as a function of the ratio to the standard model Higgs production cross section and branching fractions ($\mathcal{R}$), indicating varying degrees of overcoverage for the range $0 < \mathcal{R} < 20$ as expected for this method.

III. DERIVED UPPER LIMITS

We derive limits on SM Higgs boson production $\sigma \times BR(H \to b\bar{b}/W^+W^-)$ via 23 individual analyses [4–10]. The limits are derived at a 95% C.L. To facilitate model transparency and to accommodate analyses with different degrees of sensitivity, we present our results in terms of the ratio of 95% C.L. upper cross section limits to the SM cross section as a function of Higgs mass. The SM prediction for Higgs boson production would therefore be considered excluded at 95% C.L. when this limit ratio falls below unity. For the combined limit, the $WH \to \ell\nu b\bar{b}$ and $ZH \to \nu\bar{\nu}b\bar{b}$ signals are summed and their common background only enters the calculation once.

The individual analyses described above are grouped to evaluate combined limits over the range $105 \leq m_H \leq 200$ GeV/c^2. The $WH \to \ell\nu b\bar{b}$ and $ZH \to \ell\ell/\nu\nu b\bar{b}$ analyses contribute to the region $m_H \leq 140$ GeV/c^2, while the

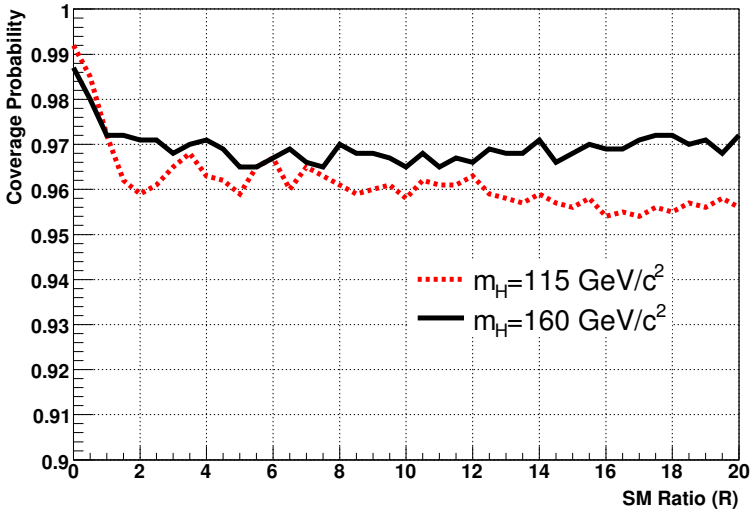

FIG. 3: Frequentist coverage probability as a function of signal cross section relative to the standard model cross section for two Higgs mass hypotheses.

TABLE II: List of leading correlated systematic uncertainties. The values for the systematic uncertainties are the same for the $ZH \to \nu\bar{\nu}b\bar{b}$ and $WH \to \ell\nu b\bar{b}$ channels. All uncertainties within a group are considered 100% correlated across channels. The correlated systematic uncertainty on the background cross section (σ) is itself subdivided according to the different background processes in each analysis.

Source	$WH \to e\nu b\bar{b}$ DT(ST)	$WH \to \mu\nu b\bar{b}$ DT(ST)	$WH \to WW^+W^-$	$H \to W^+W^-$
Luminosity (%)	6.1	6.1	-	-
Normalization (%)	-	-	6.1	4-6
Jet Energy Scale (%)	3.0	3.0	0	3.0
Jet ID (%)	3.0	3.0	-	-
Electron ID/Trigger (%)	6.0	-	11	2.3-10
Muon ID/Trigger (%)	-	11.0	11	7.7-10
b-Jet Tagging (%)	9.2(4.6)	9.2(4.6)	-	-
Background σ (%)	6-20	6-20	6-18	6-18
Signal σ (%)	0	0	0	10
QCD multijets (%)	14	14	3	15-40

Source	$ZH \to \nu\bar{\nu}b\bar{b}$	$ZH \to e^+e^-b\bar{b}$ DT(ST)	$ZH \to \mu^+\mu^-b\bar{b}$ DT(ST)
Luminosity (%)	6.1	6.1	-
Normalization (%)	-	-	6.1
Jet Energy Scale (%)	10	2.0	2.0
Jet ID (%)	5	5.0	5.0
Jet Triggers (%)	5	-	-
Electron ID/Trigger (%)	0	4.0	-
Muon ID/Trigger (%)	0	-	4.0
b-Jet Tagging (%)	7	7.5(3.0)	7.5(3.0)
Background σ (%)	6-20	10-30	10-30
QCD multijets (%)	20	50	50

$H \to W^+W^-$and $WH \to WW^+W^-$analyses contribute for $m_H \geq 120$ GeV/c^2.

Figure 4 shows the expected and observed 95% C.L. cross section limit ratio to the SM cross sections for all analyses combined in the low- and high-mass regions ($105 \leq m_H \leq 200$ GeV/c^2). The LLR distributions for the full combination are shown in Fig. 5. Included in these figures are the median LLR values for the signal-plus-background hypothesis (LLR_{s+b}), background-only hypothesis (LLR_b), and the observed data (LLR_{obs}). The shaded bands represent the 1 and 2 standard deviation (σ) departures for LLR_b. These distributions can be interpreted as follows:

- The separation between LLR_b and LLR_{s+b} provides a measure of the discriminating power of the search. This is the ability of the analysis to separate the $s+b$ and $b-$only hypotheses.

TABLE III: The correlation matrix for the analysis channels. The correlations for the $ZH \to \nu\bar{\nu}b\bar{b}$ and $WH \to \ell\nu b\bar{b}$ channels are held to be the same. All uncertainties within a group are considered 100% correlated across channels. The correlated systematic uncertainty on the background cross section (σ) is itself subdivided according to the different background processes in each analysis.

Source	$WH \to \ell\nu b\bar{b}$	$ZH \to \nu\bar{\nu}b\bar{b}$	$ZH \to \ell\ell b\bar{b}$	$H \to W^+W^-$	$WH \to WW^+W^-$
Luminosity	×	×	×		
Normalization			×	×	×
Jet Energy Scale	×	×	×	×	
Jet ID	×	×	×		
Electron ID/Trigger	×		×	×	×
Muon ID/Trigger	×		×	×	×
b-Jet Tagging	×	×	×		
Background σ	×	×	×	×	×
Signal σ				×	
QCD multijets (%)					

- The width of the LLR_b distribution (shown here as one and two standard deviation (σ) bands) provides an estimate of how sensitive the analysis is to a signal-like fluctuation in data, taking account of the presence of systematic uncertainties. For example, when a 1σ background fluctuation is large compared to the signal expectation, the analysis sensitivity is thereby limited.
- The value of LLR_{obs} relative to LLR_{s+b} and LLR_b indicates whether the data distribution appears to be more signal-like or background-like. As noted above, the significance of any departures of LLR_{obs} from LLR_b can be evaluated by the width of the LLR_b distribution.

TABLE IV: Combined 95% C.L. limits on $\sigma \times BR(H \to b\bar{b}/W^+W^-)$ for SM Higgs boson production. The limits are reported in units of the SM production cross section times branching fraction.

m_H (GeV/c^2)	105	115	125	140	160	180	200
Expected	4.4	5.8	7.5	5.7	2.8	4.4	10.5
Observed	4.5	6.4	10.9	10.2	2.6	5.0	12.7

IV. CONCLUSIONS

We have presented limits on standard model Higgs boson production derived from 23 Higgs search analyses. We have combined these analyses and form new limits more sensitive than each individual limit. The observed (expected) 95% C.L. limit ratios to the SM Higgs boson production cross sections are 6.4 (5.8) at $m_H = 115$ GeV/c^2 and 2.6 (2.8) at $m_H = 160$ GeV/c^2.

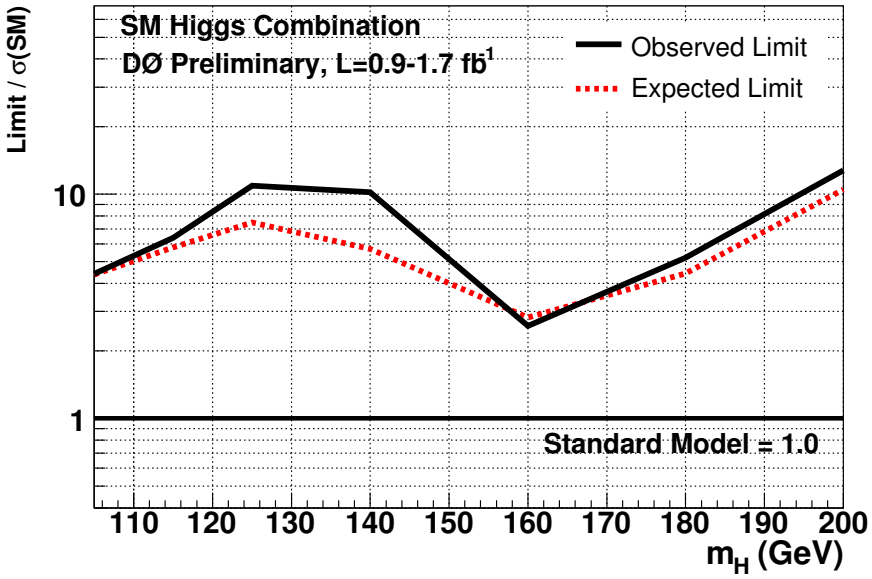

FIG. 4: Expected (median) and observed 95% C.L. cross section limit ratios for the combined $WH/ZH/H, H \to b\bar{b}/W^+W^-$ analyses over the $105 \leq m_H \leq 200$ GeV/c^2 mass range.

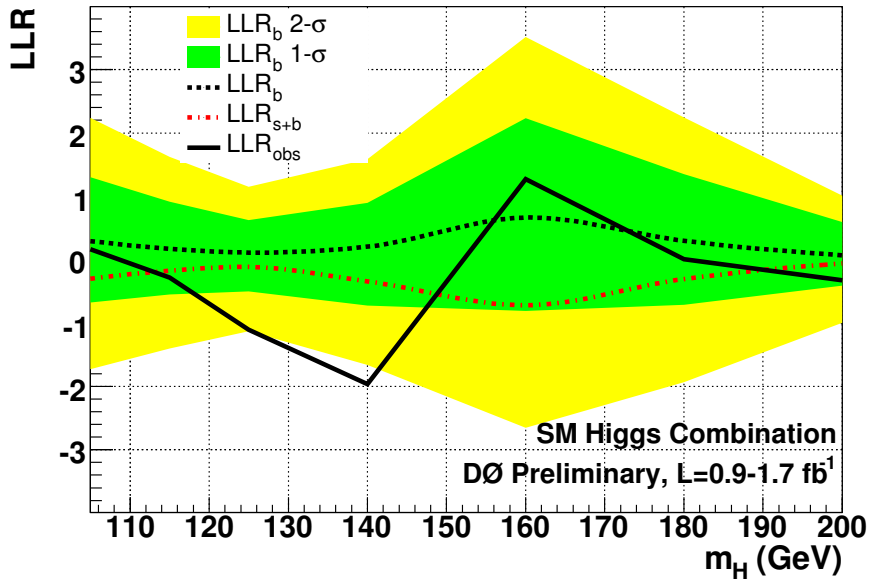

FIG. 5: Log-likelihood ratio distribution for the combined $WH/ZH/H, H \to b\bar{b}/W^+W^-$ analyses over the $105 \leq m_H \leq 200$ GeV/c^2 mass range.

Acknowledgments

We thank the staffs at Fermilab and collaborating institutions, and acknowledge support from the DOE and NSF (USA); CEA and CNRS/IN2P3 (France); FASI, Rosatom and RFBR (Russia); CAPES, CNPq, FAPERJ, FAPESP and FUNDUNESP (Brazil); DAE and DST (India); Colciencias (Colombia); CONACyT (Mexico); KRF and KOSEF (Korea); CONICET and UBACyT (Argentina); FOM (The Netherlands); PPARC (United Kingdom); MSMT (Czech Republic); CRC Program, CFI, NSERC and WestGrid Project (Canada); BMBF and DFG (Germany); SFI (Ireland);

Research Corporation, Alexander von Humboldt Foundation, and the Marie Curie Program.

---

[1] R. Barate *et al.* [LEP Working Group for Higgs boson searches], Phys. Lett. B **565**, 61 (2003), [arXiv:hep-ex/0306033].
[2] LEP Electroweak Working Group: http://lepewwg.web.cern.ch/LEPEWWG/plots/winter2007//.
[3] DØ Collaboration, V. Abazov *et. al.*, Nucl. Instrum. Meth. A **565**, 463 (2006) [arXiv:hep-ex/0507191].
[4] DØ Collaboration, DØ Note 5472-CONF.
[5] DØ Collaboration, DØ Note 5506-CONF.
[6] DØ Collaboration, DØ Note 5482-CONF.
[7] DØ Collaboration, DØ Note 5485-CONF.
[8] DØ Collaboration, DØ Note 5537-CONF.
[9] DØ Collaboration, DØ Note 5489-CONF.
[10] DØ Collaboration, DØ Note 5502-CONF.
[11] T. Scanlon, FERMILAB-THESIS-2006-43.
[12] T. Sjöstrand, P. Edén, C. Friberg, L. Lönnblad, G. Miu, S. Mrenna and E. Norrbin, Computer Phys. Commun. **135** 238 (2001) [arXiv:hep-ph/0010017].
[13] J. Pumplin *et al.*, JHEP **0207**, 012 (2002).
[14] S. Catani *et al.*, JHEP **0307**, 028 (2003) [arXiv:hep-ph/0306211].
[15] K. A. Assamagan *et al.* [Higgs Working Group Collaboration], arXiv:hep-ph/0406152.
[16] A. Djouadi, J. Kalinowski and M. Spira, Comput. Phys. Commun. **108**, 56 (1998) [arXiv:hep-ph/9704448].
[17] M. L. Mangano *et al.*, JHEP **0307**, 001 (2003) [arXiv:hep-ph/0206293].
[18] A. Pukhov *et al.*, arXiv:hep-ph/9908288.
[19] http://mcfm.fnal.gov//.
[20] T. Junk, Nucl. Intrum. Meth. A **434**, 435 (1999); A.Read, CERN 2000-005 (30 May 2000).
[21] K. S. Cranmer, Comput. Phys. Commun. **136**, 198 (2001) [arXiv:hep-ph/0011057].
[22] A. Read, Nucl. Intrum. Meth. A **425**, 357 (1999).
[23] W. Fisher, FERMILAB-TM-2386-E.